Self-Sensing Control of a PMSM used for an Automotive Application with a novel Rotor Position Estimator based on the Back-Electromotive Force

Viktor Willich and Axel Mertens
Institute for Power Electronics and Drive Systems
Leibniz University Hannover
Hanover, Germany
viktor.willich@ial.uni-hannover.de

***Abstract*—This paper presents a novel rotor position estimation method used for a permanent magnet synchronous machine (PMSM) at medium to high speeds. Through the direct evaluation of the stator voltage differential equation by means of online optimisation of a defined error function, highly responsive dynamics can be achieved. The estimation is performed synchronous to the pulse-width-modulation (PWM) period and uses two current samples per PWM period, which allows the estimation to be implemented on a commercial converter. The estimator is evaluated in simulations and experiments using a machine designed for automotive traction applications.**

***Index Terms*—Back-Electromotive Force, Permanent Magnet Synchronous Machine, Self-Sensing Control**

I. Introduction

The self-sensing control (SSC) of a permanent magnet synchronous machine (PMSM) by evaluating the back-electromotive force (EMF) has been developed over many years and several methods have been presented to estimate the rotor position and speed [1]. The evaluation of the EMF is a common approach since this is directly proportional to the machine speed, which offers the possibility of position estimation at medium and high speeds.

For EMF-based methods, different estimation principles have been developed. Estimation methods based on the extended EMF (e.g., [2], [3]) were proposed to consider the induced voltage of the permanent magnets as well as the machine's saliency. These methods offer easy implementation. In most cases, a phase-locked loop (PLL) is necessary for rotor position estimation. A PLL has the disadvantage of needing to be tuned empirically or numerically to allow a stable estimation, making the commissioning difficult.

In [4], a current oversampling approach has been developed that measures the current slopes of the individual switching states. The phase currents are sampled with a higher sampling rate compared to the pulse-width-modulation (PWM) frequency. The current samples are used for a linear regression during the switching states of the converter.

In [5], the back-electromotive force estimator with quasi-direct calculation (EMF-QD) uses this current oversampling technique in combination with a quasi-direct (QD) calculation to identify the rotor position. The QD calculation offers the advantage, in comparison to an approach using a PLL, that the parameters can be tuned analytically [6]. Highly responsive dynamics were observed for low to medium speeds. This estimation method relies on the linearity of the current slopes during the passive switching state (PS) of the converter. The use of this estimator is therefore limited to medium speeds of a machine since the PS is not present at high speeds.

Furthermore, the linearity of the current slopes cannot be assumed for all applications. The current slopes can show non-linear behaviour if the ratio of the electrical time constant to the inverter switching period is small [7]. At high speeds, the EMF can also lead to non-linear slopes [8].

The aim of this paper is to develop a method that uses the QD calculation from [5] without the need for current oversampling. The proposed estimator structure overcomes the challenges of the position estimation at high speeds, where linear current slopes cannot be assumed or the PS is too short to measure the current slope. This is achieved by using a regular current sampling technique. The proposed estimator is therefore called the back-electromotive force estimator with quasi-direct calculation using regular sampling (EMF-QD-RS).

II. Derivation of the EMF-QD-RS

In the following, the model of the PMSM in the estimated $\hat{\mathrm{d}}\hat{\mathrm{q}}$-reference frame and the adaptation law of the estimator are presented; the error function of the EMF-QD-RS is derived.

A. Model of the PMSM

The machine model is given by the stator voltage equation in the stationary $\alpha\beta$-reference frame

$$\vec{v}_{\alpha\beta} = R\vec{i}_{\alpha\beta} + \frac{\mathrm{d}\vec{\Psi}_{\alpha\beta}}{\mathrm{d}t}. \tag{1}$$

The isotropic stator resistance is defined as R, while $\vec{i}_{\alpha\beta}$ describes the stator current and $\vec{\Psi}_{\alpha\beta}$ the machine's flux linkage in the stationary $\alpha\beta$-reference frame. The derivative of

the flux linkage can be expressed in the rotating dq-reference frame

$$\frac{\mathrm{d}\vec{\Psi}_{\alpha\beta}}{\mathrm{d}t} = \frac{\mathrm{d}\mathbf{T}\vec{\Psi}_{\mathrm{dq}}}{\mathrm{d}t} \tag{2}$$

by using the transformation matrix

$$\mathbf{T} = \begin{pmatrix} \cos(\gamma_{\mathrm{el}}) & -\sin(\gamma_{\mathrm{el}}) \\ \sin(\gamma_{\mathrm{el}}) & \cos(\gamma_{\mathrm{el}}) \end{pmatrix} \tag{3}$$

with γ_{el} being the electrical rotor angle. Inserting (2) into (1) and applying the product rule to the derivative of the flux results in

$$\begin{aligned} \vec{v}_{\alpha\beta} &= R\vec{i}_{\alpha\beta} + \frac{\mathrm{d}\mathbf{T}\vec{\Psi}_{\mathrm{dq}}}{\mathrm{d}t} \\ &= R\vec{i}_{\alpha\beta} + \mathbf{T}\frac{\mathrm{d}\vec{\Psi}_{\mathrm{dq}}}{\mathrm{d}t} + \frac{\mathrm{d}\mathbf{T}}{\mathrm{d}t}\vec{\Psi}_{\mathrm{dq}} \\ &= R\vec{i}_{\alpha\beta} + \mathbf{T}\frac{\mathrm{d}\vec{\Psi}_{\mathrm{dq}}}{\mathrm{d}\vec{i}_{\mathrm{dq}}}\frac{\mathrm{d}\vec{i}_{\mathrm{dq}}}{\mathrm{d}t} + \frac{\mathrm{d}\mathbf{T}}{\mathrm{d}t}\vec{\Psi}_{\mathrm{dq}}. \end{aligned} \tag{4}$$

The flux can be separated into the flux $\vec{\Psi}_{\mathrm{L,dq}}$ which is produced by the stator currents and the flux $\vec{\Psi}_{\mathrm{PM,dq}}$ due to the permanent magnets in the rotor

$$\begin{aligned} \vec{\Psi}_{\mathrm{dq}} &= \vec{\Psi}_{\mathrm{L,dq}} + \vec{\Psi}_{\mathrm{PM,dq}} \\ &= \mathbf{L}_{\mathrm{dq}}(\vec{i}_{\mathrm{dq}})\vec{i}_{\mathrm{dq}} + \begin{pmatrix} \Psi_{\mathrm{PM}} \\ 0 \end{pmatrix}. \end{aligned} \tag{5}$$

The derivative of the flux in the rotating dq-reference frame in the direction of the dq-currents is defined as being the current-dependent differential inductance matrix $\mathbf{L}'_{\mathrm{dq}}$, while $\mathbf{L}_{\mathrm{dq}}$ represents the current-dependent secant inductance matrix

$$\mathbf{L}'_{\mathrm{dq}}(\vec{i}_{\mathrm{dq}}) = \begin{pmatrix} L'_{\mathrm{d}}(\vec{i}_{\mathrm{dq}}) & L'_{\mathrm{dq}}(\vec{i}_{\mathrm{dq}}) \\ L'_{\mathrm{dq}}(\vec{i}_{\mathrm{dq}}) & L'_{\mathrm{q}}(\vec{i}_{\mathrm{dq}}) \end{pmatrix} = \begin{pmatrix} \frac{\partial\Psi_{\mathrm{d}}}{\partial i_{\mathrm{d}}} & \frac{\partial\Psi_{\mathrm{d}}}{\partial i_{\mathrm{q}}} \\ \frac{\partial\Psi_{\mathrm{q}}}{\partial i_{\mathrm{d}}} & \frac{\partial\Psi_{\mathrm{q}}}{\partial i_{\mathrm{q}}} \end{pmatrix} \tag{6}$$

$$\mathbf{L}_{\mathrm{dq}}(\vec{i}_{\mathrm{dq}}) = \begin{pmatrix} L_{\mathrm{d}}(\vec{i}_{\mathrm{dq}}) & L_{\mathrm{dq}}(\vec{i}_{\mathrm{dq}}) \\ L_{\mathrm{dq}}(\vec{i}_{\mathrm{dq}}) & L_{\mathrm{q}}(\vec{i}_{\mathrm{dq}}) \end{pmatrix} = \begin{pmatrix} \frac{\Psi_{\mathrm{d}}}{i_{\mathrm{d}}} & \frac{\Psi_{\mathrm{d}}}{i_{\mathrm{q}}} \\ \frac{\Psi_{\mathrm{q}}}{i_{\mathrm{d}}} & \frac{\Psi_{\mathrm{q}}}{i_{\mathrm{q}}} \end{pmatrix}. \tag{7}$$

The derivative of the transformation matrix (3) yields

$$\frac{\mathrm{d}\mathbf{T}}{\mathrm{d}t} = \mathbf{J}\omega_{\mathrm{el}}\mathbf{T} \tag{8}$$

where ω_{el} represents the electrical angular frequency. Inserting (5), (6) and (8) into (4) and expressing the currents in the $\alpha\beta$-reference frame results in

$$\begin{aligned} \vec{v}_{\alpha\beta} &= R\vec{i}_{\alpha\beta} + \mathbf{T}\mathbf{L}'_{\mathrm{dq}}\frac{\mathrm{d}\vec{i}_{\mathrm{dq}}}{\mathrm{d}t} + \mathbf{J}\omega_{\mathrm{el}}\mathbf{T}\mathbf{L}_{\mathrm{dq}}\vec{i}_{\mathrm{dq}} + \mathbf{J}\omega_{\mathrm{el}}\mathbf{T}\vec{\Psi}_{\mathrm{PM,dq}} \\ &= R\vec{i}_{\alpha\beta} + \mathbf{T}\mathbf{L}'_{\mathrm{dq}}\frac{\mathrm{d}\mathbf{T}^{-1}\vec{i}_{\alpha\beta}}{\mathrm{d}t} + \mathbf{J}\omega_{\mathrm{el}}\mathbf{T}\mathbf{L}_{\mathrm{dq}}\mathbf{T}^{-1}\vec{i}_{\alpha\beta} \\ &\quad + \mathbf{J}\omega_{\mathrm{el}}\mathbf{T}\vec{\Psi}_{\mathrm{PM,dq}} \\ &= R\vec{i}_{\alpha\beta} + \mathbf{L}'_{\alpha\beta}\frac{\mathrm{d}\vec{i}_{\alpha\beta}}{\mathrm{d}t} + \left(\mathbf{J}\mathbf{L}_{\alpha\beta} - \mathbf{L}'_{\alpha\beta}\mathbf{J}\right)\omega_{\mathrm{el}}\vec{i}_{\alpha\beta} \\ &\quad + \mathbf{J}\omega_{\mathrm{el}}\vec{\Psi}_{\mathrm{PM},\alpha\beta} \end{aligned} \tag{9}$$

and describes the non-linear stator voltage equation in the stationary $\alpha\beta$-reference frame.

B. Quasi-Direct Calculation

A significant difference of the EMF-QD-RS compared to other EMF-based estimation methods is the use of the QD calculation in connection with a regular current sampling. The rotor angle estimation error is defined as

$$\gamma_{\mathrm{err}} = \gamma_{\mathrm{el}} - \hat{\gamma}_{\mathrm{el}} \tag{10}$$

with $\hat{\gamma}_{\mathrm{el}}$ being the estimated rotor position.

Analogous to [5] and [9], the adaptation law of the QD calculation is derived using the gradient descent method (GDM). An error function is defined using the stator voltage differential equation which is minimised through selection of the optimum value of the estimated rotor angle estimation error $\hat{\gamma}_{\mathrm{err}}$. The defined error function is defined as being

$$E = \frac{1}{2}\vec{e}(\hat{\gamma}_{\mathrm{err}})^T\vec{e}(\hat{\gamma}_{\mathrm{err}}). \tag{11}$$

To minimise the error function, the gradient

$$g = \vec{e}(\hat{\gamma}_{\mathrm{err}})^T \cdot \frac{\partial\vec{e}(\hat{\gamma}_{\mathrm{err}})}{\partial\hat{\gamma}_{\mathrm{err}}} \tag{12}$$

in the direction of the rotor angle estimation error $\hat{\gamma}_{\mathrm{err}}$ is calculated. The QD calculation is based on multiple calculations of the error function with a varying value for $\hat{\gamma}_{\mathrm{err}}$. This ensures the minimisation of the error function for each call of the estimator. For each iteration, the gradient (12) is calculated using the estimated value for $\hat{\gamma}_{\mathrm{err}}$, which is then used to adapt the parameter according to

$$\hat{\gamma}_{\mathrm{err}}(i+1) = \hat{\gamma}_{\mathrm{err}}(i) - \eta \cdot \mathrm{sgn}(g(i)) \tag{13}$$

with η being the step width of the QD calculation [10]. This ensures the correct estimation during each call of the estimator. The variable i is the iteration counter of the tracker.

C. Derivation of the Error Function

The error function which is optimised through the QD calculation is based on the non-linear stator voltage Equation (9). Since the rotor angle γ_{el} is not known, Equation (9) is transformed into the estimated $\hat{\mathrm{d}}\hat{\mathrm{q}}$-reference frame. This is done using the transformation matrix

$$\hat{\mathbf{T}}^{-1} = \begin{pmatrix} \cos(\hat{\gamma}_{\mathrm{el}}) & \sin(\hat{\gamma}_{\mathrm{el}}) \\ -\sin(\hat{\gamma}_{\mathrm{el}}) & \cos(\hat{\gamma}_{\mathrm{el}}) \end{pmatrix}. \tag{14}$$

The transformation results in

$$\begin{aligned} \vec{v}_{\hat{\mathrm{d}}\hat{\mathrm{q}}} &= \hat{\mathbf{T}}^{-1}\vec{v}_{\alpha\beta} \\ &= \hat{\mathbf{T}}^{-1}R\hat{\mathbf{T}}\vec{i}_{\hat{\mathrm{d}}\hat{\mathrm{q}}} + \hat{\mathbf{T}}^{-1}\mathbf{T}\mathbf{L}'_{\mathrm{dq}}\mathbf{T}^{-1}\frac{\mathrm{d}\hat{\mathbf{T}}\vec{i}_{\hat{\mathrm{d}}\hat{\mathrm{q}}}}{\mathrm{d}t} \\ &\quad + \hat{\mathbf{T}}^{-1}\left(\mathbf{J}\mathbf{T}\mathbf{L}_{\mathrm{dq}}\mathbf{T}^{-1} - \mathbf{T}\mathbf{L}'_{\mathrm{dq}}\mathbf{T}^{-1}\mathbf{J}\right)\omega_{\mathrm{el}}\hat{\mathbf{T}}\vec{i}_{\hat{\mathrm{d}}\hat{\mathrm{q}}} \\ &\quad + \hat{\mathbf{T}}^{-1}\mathbf{J}\omega_{\mathrm{el}}\mathbf{T}\vec{\Psi}_{\mathrm{dq}} \\ &= R\vec{i}_{\hat{\mathrm{d}}\hat{\mathrm{q}}} + \tilde{\mathbf{T}}^{-1}\mathbf{L}'_{\mathrm{dq}}\tilde{\mathbf{T}}\frac{\mathrm{d}\vec{i}_{\hat{\mathrm{d}}\hat{\mathrm{q}}}}{\mathrm{d}t} + \tilde{\mathbf{T}}^{-1}\mathbf{J}\omega_{\mathrm{el}}\mathbf{L}_{\mathrm{dq}}\tilde{\mathbf{T}}\vec{i}_{\hat{\mathrm{d}}\hat{\mathrm{q}}} \\ &\quad + \omega_{\mathrm{el}}\tilde{\mathbf{T}}^{-1}\hat{\Psi}_{\mathrm{PM}} \\ &= R\vec{i}_{\hat{\mathrm{d}}\hat{\mathrm{q}}} + \mathbf{L}'_{\hat{\mathrm{d}}\hat{\mathrm{q}}}\frac{\mathrm{d}\vec{i}_{\hat{\mathrm{d}}\hat{\mathrm{q}}}}{\mathrm{d}t} + \mathbf{J}\omega_{\mathrm{el}}\mathbf{L}_{\hat{\mathrm{d}}\hat{\mathrm{q}}}\vec{i}_{\hat{\mathrm{d}}\hat{\mathrm{q}}} + \omega_{\mathrm{el}}\hat{\Psi}_{\mathrm{PM}}. \end{aligned} \tag{15}$$

The transformation matrix $\tilde{\mathbf{T}}$ represents a coordinate rotation through γ_{err}, which corresponds to a misalignment of the real and estimated rotating reference frames and is given by

$$\tilde{\mathbf{T}} = \begin{pmatrix} \cos(\gamma_{\mathrm{err}}) & \sin(\gamma_{\mathrm{err}}) \\ -\sin(\gamma_{\mathrm{err}}) & \cos(\gamma_{\mathrm{err}}) \end{pmatrix}. \tag{16}$$

By assuming small values for γ_{err}, the inductance matrices $\mathbf{L}'_{\hat{\mathrm{d}}\hat{\mathrm{q}}}$ and $\mathbf{L}_{\hat{\mathrm{d}}\hat{\mathrm{q}}}$ can be linearised to become

$$\begin{aligned}\mathbf{L}'_{\hat{\mathrm{d}}\hat{\mathrm{q}}} = &\begin{pmatrix} L'_{\mathrm{d}} & L'_{\mathrm{dq}} \\ L'_{\mathrm{dq}} & L'_{\mathrm{q}} \end{pmatrix} + \Delta L' \begin{pmatrix} 0 & 2\gamma_{\mathrm{err}} \\ 2\gamma_{\mathrm{err}} & 0 \end{pmatrix} \\ &+ L'_{\mathrm{dq}} \begin{pmatrix} -2\gamma_{\mathrm{err}} & 0 \\ 0 & 2\gamma_{\mathrm{err}} \end{pmatrix}\end{aligned} \tag{17}$$

and

$$\begin{aligned}\mathbf{L}_{\hat{\mathrm{d}}\hat{\mathrm{q}}} = &\begin{pmatrix} L_{\mathrm{d}} & L_{\mathrm{dq}} \\ L_{\mathrm{dq}} & L_{\mathrm{q}} \end{pmatrix} + \Delta L \begin{pmatrix} 0 & 2\gamma_{\mathrm{err}} \\ 2\gamma_{\mathrm{err}} & 0 \end{pmatrix} \\ &+ L_{\mathrm{dq}} \begin{pmatrix} -2\gamma_{\mathrm{err}} & 0 \\ 0 & 2\gamma_{\mathrm{err}} \end{pmatrix}\end{aligned} \tag{18}$$

with

$$\Delta L' = \frac{L'_{\mathrm{d}} - L'_{\mathrm{q}}}{2} \text{ and } \Delta L = \frac{L_{\mathrm{d}} - L_{\mathrm{q}}}{2}. \tag{19}$$

The estimated flux linkage $\hat{\Psi}_{\mathrm{PM}}$ is given by

$$\hat{\Psi}_{\mathrm{PM}} = \begin{pmatrix} -\gamma_{\mathrm{err}} \\ 1 \end{pmatrix} \Psi_{\mathrm{PM}}. \tag{20}$$

Since the optimisation evaluates only the gradient in the direction of $\hat{\gamma}_{\mathrm{err}}$, the voltage terms that have a dependency on this variable carry the rotor position information. As it can be seen from (15), there are several terms that are dependent on this value. In order to simplify the estimation, the terms that are dependent on $\hat{\gamma}_{\mathrm{err}}$ are only evaluated if they are proportional to the angular frequency ω_{el}. The assumption is made, that the angular frequency has no estimation error, so that $\hat{\omega}_{\mathrm{el}}$ can be used in Equation (15). To further simplify the error equation, only the $\hat{\mathrm{d}}$-axis is evaluated in the QD calculation.

The error equation results in

$$\begin{aligned}e_{\hat{\mathrm{d}}} = &Ri_{\hat{\mathrm{d}}} + L'_{\mathrm{d}}\frac{\mathrm{d}i_{\hat{\mathrm{d}}}}{\mathrm{d}t} + L'_{\mathrm{dq}}\frac{\mathrm{d}i_{\hat{\mathrm{q}}}}{\mathrm{d}t} - L_{\mathrm{dq}}\hat{\omega}_{\mathrm{el}}i_{\hat{\mathrm{d}}} - L_{\mathrm{q}}\hat{\omega}_{\mathrm{el}}i_{\hat{\mathrm{q}}} \\ &- v^*_{\hat{\mathrm{d}}} - \hat{\gamma}_{\mathrm{err}}\hat{\omega}_{\mathrm{el}}\left(2\Delta L i_{\hat{\mathrm{d}}} + 2L_{\mathrm{dq}}i_{\hat{\mathrm{q}}} + \Psi_{\mathrm{PM}}\right).\end{aligned} \tag{21}$$

The voltage $v^*_{\hat{\mathrm{d}}}$ used in (21) is the voltage setpoint coming from the current regulator of the $\hat{\mathrm{d}}$-axis.

The partial derivative of (21) with respect to $\hat{\gamma}_{\mathrm{err}}$ is

$$\frac{\partial e_{\hat{\mathrm{d}}}}{\partial \hat{\gamma}_{\mathrm{err}}} = -\hat{\omega}_{\mathrm{el}}\left(2\Delta L i_{\hat{\mathrm{d}}} + 2L_{\mathrm{dq}}i_{\hat{\mathrm{q}}} + \Psi_{\mathrm{PM}}\right). \tag{22}$$

The resulting calculation of the gradient for each iteration i is shown in Fig. 1

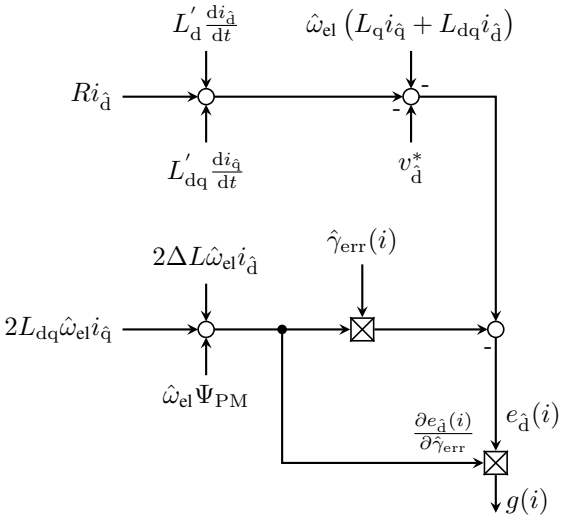

Fig. 1: Resulting structure of the adaption law for one iteration

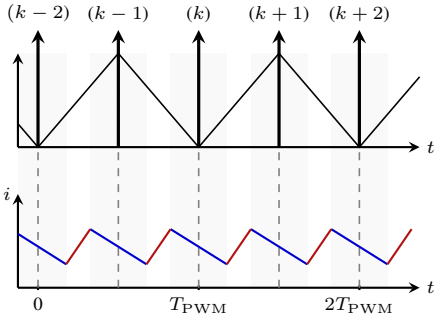

Fig. 2: PWM-synchronous current sampling methods commonly used in commercial drive systems with sampling instances at the top and the bottom of the carrier waveform

D. Implementation of the EMF-QD-RS

A significant difference from the estimator structure proposed in [5] is the PWM-synchronous sampling technique as this is commonly used in drive systems to eliminate the switching harmonics in the current [7].

For the implementation, the currents are sampled twice per PWM cycle, synchronously to the carrier waveform. In Fig. 2, the sampling instances are shown with respect to the switching period and the current slope for a random operating point. Each sampling instance is indicated by the number k. Due to the sampling instances being chosen at the top and bottom of the carrier waveform, the sampling coincides with the centre of each PS of the inverter, which corresponds to the mean value of the sampled current of each PWM interval. By using this regular sampling scheme, the fundamental currents can be measured and used for field-oriented control (FOC) and rotor position estimation.

The current derivatives used for the error equation (21) are calculated as

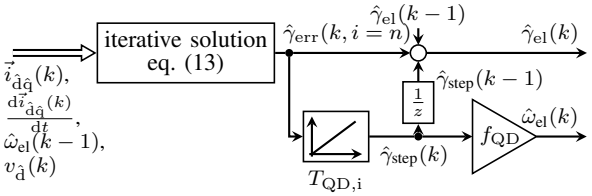

Fig. 3: Estimator structure of the EMF-QD-RS (cf. [5])

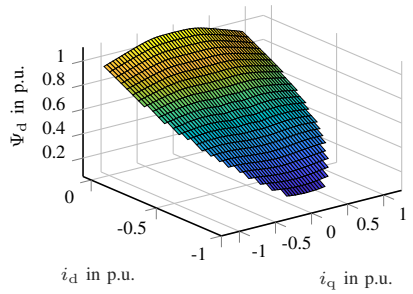

Fig. 4: Flux linkage of the d-axis relative to the operating ranges of i_{d} and i_{q}

$$\frac{\mathrm{d}\vec{i}_{\hat{\mathrm{d}}\hat{\mathrm{q}}}(k)}{\mathrm{d}t} = \frac{\vec{i}_{\hat{\mathrm{d}}\hat{\mathrm{q}}}^{(k)} - \vec{i}_{\hat{\mathrm{d}}\hat{\mathrm{q}}}^{(k-1)}}{\frac{T_{\mathrm{PWM}}}{2}}. \tag{23}$$

The resulting estimator structure is shown in Fig. 3. At each call of the estimator, the input values are acquired from the current sensors and controller. With these inputs, the gradient $g(i)$ is calculated for each iteration using (12) and the result is then used to adapt the estimation error $\hat{\gamma}_{\mathrm{err}}$ according to (13). This adaptation is carried out for a fixed number of iterations. The resulting $\hat{\gamma}_{\mathrm{err}}$ is then fed to an integrator with the time constant $T_{\mathrm{QD,i}}$. The integrator output $\hat{\gamma}_{\mathrm{step}}$ is used for speed estimation by multiplying it with the calling rate f_{QD} of the estimator [10]. The estimated rotor angle is finally calculated by adding the identified estimated value $\hat{\gamma}_{\mathrm{err}}$ to the integrator output $\hat{\gamma}_{\mathrm{step}}$ and the estimated rotor angle from the previous estimator call.

III. Validation of the Estimator

The EMF-QD-RS has been tested in simulations and was implemented on an experimental test bench for validation purposes. The machine used for the SSC is a PMSM which is used for an automotive traction application. This machine has an output power of about 80 kW in the constant power operation. At different operating points, the machine experiences strong saturation effects. The flux linkages in the dq-reference frame can be seen in Fig. 4 and Fig. 5. The flux linkages in these figures are normalised with respect to the flux linkage of the permanent magnets at no-load operation.

Due to the saturation, the effective inductances of the machine are dependent on the operating point of the machine.

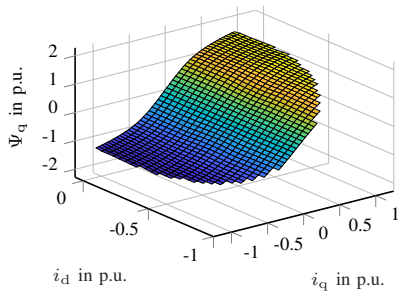

Fig. 5: Flux linkage of the q-axis relative to the operating ranges of i_{d} and i_{q}

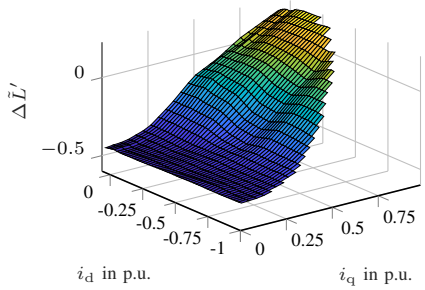

Fig. 6: Relative saliency $\Delta\tilde{L}'$ of the differential machine inductances over the operating ranges of i_{d} and i_{q}

The relative differential saliency of the machine is given by

$$\Delta\tilde{L}' = \frac{L_{\mathrm{d}}' - L_{\mathrm{q}}'}{L_{\mathrm{d}}' + L_{\mathrm{q}}'}. \tag{24}$$

and shown in Fig. 6. It can be seen that the machine inductances in the dq-reference frame are subject to strong saturation effects and that operating points could exist where the saliency is equal to zero. The influence of the saturation on the inductance matrix needs to be considered for the estimation in order to provide a high quality rotor position estimation under all load conditions. For this reason, the inductances used for position estimation are adapted according their dependency on the stator currents $\vec{i}_{\mathrm{dq}}$.

The control structure used for simulation and experimental validation is shown in Fig. 7. In this structure, the rotor angle used for the FOC is estimated by the EMF-QD-RS. The angular frequency is estimated according to the iterative structure shown in Fig. 3.

As is common for automotive traction applications, the machine under test is controlled to provide a torque. The torque setpoint M^* and the angular frequency $\hat{\omega}_{\mathrm{el}}$ are converted to the current setpoints in the dq-reference frame by means of a lookup table (LUT) which represents the optimum efficiency operation of the machine. The current controller is implemented using a PI Controller for the d- and q-axis currents. In order to control the speed of the machine, a load machine is coupled which is controlled to provide a fixed speed. The load

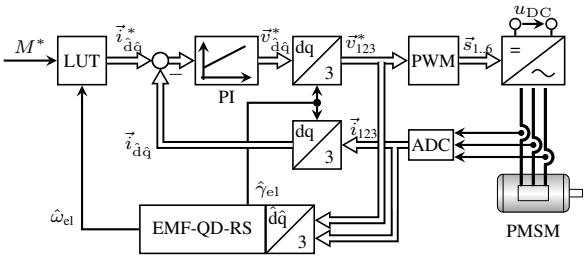

Fig. 7: Control structure of the machine under test including the EMF-QD-RS for rotor angle and speed estimation

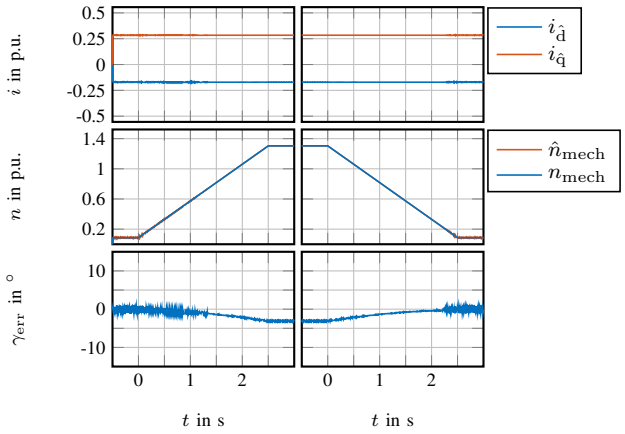

Fig. 8: Simulation results of the SSC using the EMF-QD-RS during an acceleration from a speed of 0.1 p.u. to a speed of 1.36 p.u. while the machine under test is controlled to provide a torque of 0.3 p.u.

machine is therefore providing the mechanical speed while the traction machine applies a torque to the shaft.

In the following, the electrical parameters of the machine are normalised with respect to the parameters relating to constant power operation of the machine at rated speed.

A. Simulation Results

The rotor angle estimation of the EMF-QD-RS is tested under different operating conditions of the machine. Two test scenarios are defined to evaluate the dynamic behaviour of the estimation.

For the investigation of the dynamic behaviour of the estimator during speed transients, a torque of 0.3 p.u. is applied while the speed is linearly changed by the load machine from 0.1 p.u. to 1.3 p.u. Figure 8 shows the dynamic behaviour during the change in speed. On the right-hand side, the corresponding deceleration is shown. The SSC works in closed loop during these tests, which means that the estimated position and speed are used for feedback. The currents in the $\hat{\mathrm{d}}\hat{\mathrm{q}}$-reference frame, as well as the mechanical speed, the estimated speed and the resulting electrical rotor angle estimation error γ_{err}, are shown and analysed.

It can be seen that the estimation error γ_{err} shows harmonic oscillations at low speeds. These oscillations do not exceed a

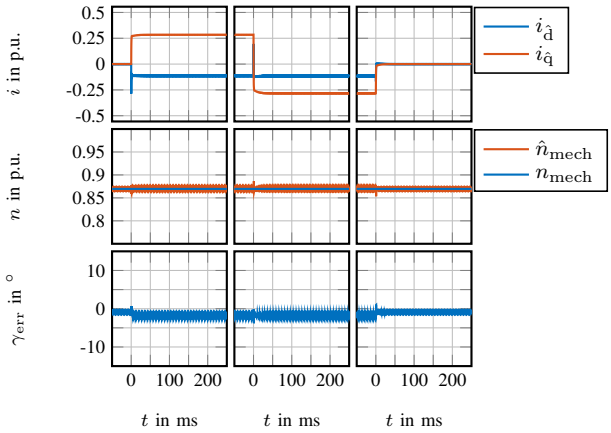

Fig. 9: Simulation results of the SSC using the EMF-QD-RS at a constant speed of 0.86 p.u. while a torque of 0.3 p.u. is applied (left), reversed (center) and set back to zero (right)

value of 3° and are therefore small enough to offer a stable control using the estimated angle. At $t = 0.5\,\mathrm{s}$, a linear speed ramp is applied and the oscillations of the estimation error decrease. At the speed of 1.36 p.u., the rotor estimation error shows a stationary offset of around $-3°$. The reverse behaviour can be seen in the deceleration process.

For the torque step response of the estimator, the speed of the machine is kept constant at approximately 0.86 p.u. while a torque setpoint of 0.3 p.u. is applied, reversed and set back to zero. The resulting estimation dynamics are shown in Fig. 9.

A good dynamic estimation behaviour can be observed while the torque steps are applied. When the machine is operating with a torque setpoint of zero, the estimation error γ_{err} is very small. During the transient states after the torque setpoint is applied, the estimation error shows no fluctuation due to the load change and ensures a stable control for dynamic torque setpoint changes. However, when the torque is applied, the estimation error experiences oscillations which are smaller than 3° in amplitude.

It can be seen that the EMF-QD-RS offers good rotor angle estimation even during sudden torque setpoint steps and ensures a stable SSC.

B. Experimental Validation

The test scenarios applied to the drive system in simulations are repeated on an experimental testbench in order to validate the results. The test bench uses a prototype traction drive system which includes a rapid prototyping system consisting of a Xilinx Zynq 7000 System on Chip (SoC) module, which combines an ARM Dual Core Cortex A9 processor and an Artix-7 FPGA. This programmable logic (PL) is used to implement the estimator structure. The inverter contains SiC MOSFET power modules for automotive applications and the system uses current sensors with a bandwidth of 500 kHz. For the evaluation of the estimation, the estimated rotor angle is

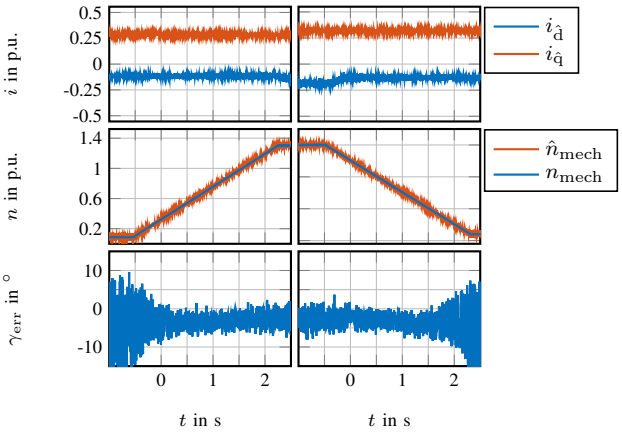

Fig. 10: Experimental results of the SSC with the EMF-QD-RS during an acceleration (left) and deceleration (right) from 0.1 p.u. to 1.36 p.u. while the machine under test applies a torque of 0.3 p.u.

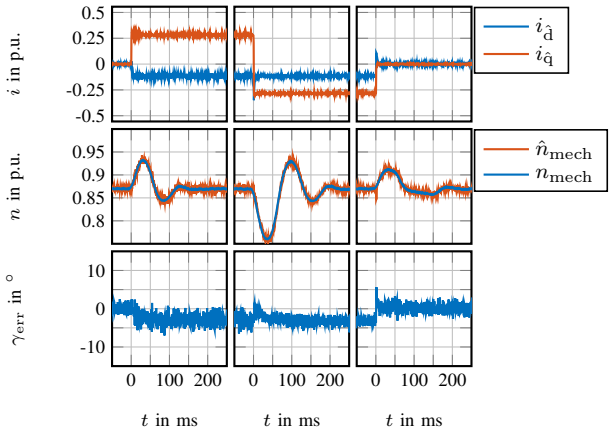

Fig. 11: Experimental results of SSC using the EMF-QD-RS for the load step response. The machine is rotating at a speed of 0.86 p.u. when a sudden load step from 0 p.u. to 0.3 p.u. is applied (left), reversed (centre) and set back to zero (right)

compared to the measurement of a resolver mounted on the machine under test.

In Fig. 11, the results of the SSC using the EMF-QD-RS are shown for the acceleration and deceleration instigated by the load machine while a constant torque of 0.3 p.u. is provided by the device under test. This represents the same test scenario evaluated in the simulations depicted in Fig. 8.

During the speed change of the machine, similar estimation behaviour compared to the simulations seen in Fig. 8 are examined. When the machine rotates at a low speed, the rotor angle estimation error γ_{err} shows oscillations with an amplitude of roughly 10°. As the machine accelerates, the estimation error decreases and reaches a value below 3°. During the deceleration, the same behaviour can be observed. The increasing estimation error at low speeds can be explained by the dependency of the error $e_{\hat{\mathrm{d}}}$ on the angular frequency $\hat{\omega}_{\mathrm{el}}$.

The system response of the SSC for sudden torque setpoint steps is shown in Fig. 11. The test scenario is chosen accordingly to the simulations so that the load machine is controlled to a speed of 0.86 p.u. while the machine under test provides the torque setpoints at $t = 0\,\mathrm{s}$. On the left, a torque of 0.3 p.u. is applied, which is then reversed to -0.3 p.u. in the centre. Finally, the torque is set back to zero, which is seen on the right-hand side of Fig. 11.

The experimental validation for the torque setpoint steps using the EMF-QD-RS shows good estimation accuracy for stationary and dynamic conditions. The rotor angle estimation error shows high accuracy during the transient states of the torque change. During the torque changes, a small transient can be observed in the estimation error γ_{err}. These transients are small and the error is below 10° at all times. During stationary operation after a torque is applied, a small offset can be seen in the estimation error. This offset can be explained by saturation effects in the machine and deviations between the effective and assumed inductances at these operating points.

After a torque setpoint step, the machine shows a significant change in speed which is caused by the torque applied to the system. The load machine reacts to the speed deviation and eventually eliminates this deviation. The measured and estimated speeds reflect this balancing process and underline the accuracy of the speed estimation during the transients.

As can be seen from the simulation and test results, the EMF-QD-RS is able to estimate the rotor position and angular frequency with high accuracy, allowing the SSC to respond to torque command steps with highly responsive dynamics. The estimation is also able to identify the rotor position and speed accurately during speed transients.

IV. Evaluation of Lower Speed Limit using the EMF-QD-RS

To analyse the operating range across which the EMF-QD-RS can be used for SSC, the lower speed limit is evaluated. As was seen in simulations and the experimental validation, the accuracy of the estimation of the rotor angle deteriorates when the machine's speed is low. In low speed operation, the error defined in (21) is very small so that the influence of the rotor position estimation error in the error function decreases at low speeds. When the influence of the estimation error gets too small, the EMF-QD-RS is not able to identify the rotor angle accurately. Since the error function becomes small at low speeds, inaccuracy of measurements and parameters can cause instability of the estimation.

The practical low speed limit for the SSC of the machine under test is experimentally evaluated by gradually reducing the speed setpoint of the load machine while the torque setpoint of the machine under test is set to zero. As the $\hat{\mathrm{d}}\hat{\mathrm{q}}$-currents are controlled to be zero, only the influence of the induced voltage from the flux linkage of the permanent magnets $\hat{\Psi}_{\mathrm{PM}}$ is evaluated (cf. (21)). Fig. 12 shows the experimental results from this evaluation. The machine's speed is reduced, starting at a few percent of the rated speed, as this is

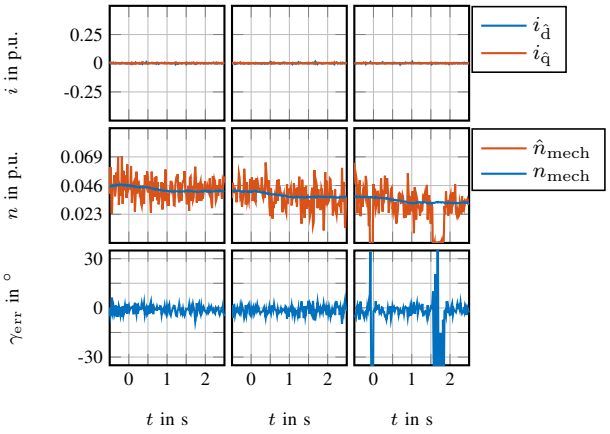

Fig. 12: Experimental evaluation of the practical low speed limit of the SSC using the EMF-QD-RS by reducing the machine's speed from 0.046 p.u. to 0.04 p.u. (left), to 0.036 p.u. (centre) and to 0.032 p.u. (right) while the torque setpoint is kept at zero.

known to be a typical limit for estimation methods evaluating the EMF [1]. The speed is reduced from 0.046 p.u. to 0.03 p.u. in three steps.

It can be seen that the SSC is stable for the first two speed reduction steps. During the last speed step from 0.036 p.u. to 0.03 p.u. at $t = 0\,\mathrm{s}$, the estimation error rises above 30°, which is selected as the termination criterion for the SSC; in which case the rotor angle of the mounted resolver is used as feedback for the FOC. This is done to ensure a stable control during operation even if the estimator is unable to determine the rotor angle.

The speed of 0.036 p.u. is therefore experimentally proven to be the low speed limit of the EMF-QD-RS for this application. It shows a good estimation behaviour up to only a few percent of the machine's rated speed.

V. Conclusion

The proposed estimator developed in this paper uses regular current sampling in combination with a QD calculation. It can estimate the rotor position and speed at medium and high speeds and shows good dynamic behaviour.

The regular current sampling makes the estimator applicable for drive systems where current oversampling and linear regression of the current slopes cannot be applied. Compared to estimators using a PLL, the QD calculation can be tuned analytically, which allows for easy commissioning of the SSC. In addition, it offers the advantage that the position can be estimated within one sampling cycle, whereas multiple sampling cycles are required when using a PLL.

Due to the use of the QD calculation, the estimator is compatible with the estimators proposed in [5] and [9]. The combination of these estimators will form the subject of future works.

References

[1] S.-K. Sul, Y.-C. Kwon, and Y. Lee, "Sensorless control of ipmsm for last 10 years and next 5 years," *CES Transactions on Electrical Machines and Systems*, vol. 1, no. 2, pp. 91–99, 2017.

[2] S. Morimoto, K. Kawamoto, M. Sanada, and Y. Takeda, "Sensorless control strategy for salient-pole pmsm based on extended emf in rotating reference frame," *IEEE Transactions on Industry Applications*, vol. 38, no. 4, pp. 1054–1061, 2002.

[3] H. Köpken, "Wide bandwidth sensorless position control using a superimposed synchronous test signal," in *2003 10th European Conference on Power Electronics and Applications (EPE'03 ECCE Europe)*, 2003.

[4] B. Weber, G. Lindemann, and A. Mertens, "Reduced observer for anisotropy-based position estimation of PM synchronous machines using current oversampling," in *2017 IEEE International Symposium on Sensorless Control for Electrical Drives (SLED)*, Sep. 2017, pp. 121–126.

[5] G. Lindemann, V. Willich, and A. Mertens, "Novel quasi-direct rotor position estimator for permanent magnet synchronous machines based on the back-electromotive force using current oversampling," in *2022 24th European Conference on Power Electronics and Applications (EPE'22 ECCE Europe)*, 2022, pp. 1–10.

[6] N. Himker and A. Mertens, "Analytical design of self-sensing control for pmsm using quasi-direct calculation," *IEEE Open Journal of Industry Applications*, pp. 1–12, 2023.

[7] F. Briz, D. Díaz-Reigosa, M. W. Degner, P. García, and J. M. Guerrero, "Current sampling and measurement in PWM operated AC drives and power converters," in *The 2010 International Power Electronics Conference*, Jun. 2010, pp. 2753–2760.

[8] J. Jacob, S. Calligaro, and R. Petrella, "Systematic current measurement error due to back-emf in pmsm drives adopting synchronous sampling," in *2018 IEEE Energy Conversion Congress and Exposition (ECCE)*, 2018, pp. 3442–3448.

[9] N. Himker, G. Lindemann, K. Wiedmann, B. Weber, and A. Mertens, "A family of adaptive position estimators for pmsm using the gradient descent method," *IEEE Journal of Emerging and Selected Topics in Power Electronics*, vol. 10, no. 2, pp. 1946–1962, 2022.

[10] N. Himker, G. Lindemann, and A. Mertens, "Iterative tracker for anisotropy-based self-sensing control of pmsm," in *2019 IEEE 10th International Symposium on Sensorless Control for Electrical Drives (SLED)*, 2019, pp. 1–6.